Clustering, collision, and relaxation dynamics in pure and doped helium nanoclusters: Density- vs particle-based approaches

Ernesto García-Alfonso, Manuel Barranco, David A. Bonhommeau, Nadine Halberstadt, Martí Pi, Florent Calvo

The Journal of Chemical Physics

Clustering, collision, and relaxation dynamics in pure and doped helium nanoclusters: Density- vs particle-based approaches

Cite as: J. Chem. Phys. **157**, 014106 (2022); https://doi.org/10.1063/5.0091942
Submitted: 18 March 2022 • Accepted: 14 June 2022 • Published Online: 05 July 2022

Ernesto García-Alfonso, Manuel Barranco, David A. Bonhommeau, et al.

The Journal of Chemical Physics ARTICLE scitation.org/journal/jcp

Clustering, collision, and relaxation dynamics in pure and doped helium nanoclusters: Density- vs particle-based approaches

Cite as: J. Chem. Phys. 157, 014106 (2022); doi: 10.1063/5.0091942
Submitted: 18 March 2022 • Accepted: 14 June 2022 •
Published Online: 5 July 2022

Ernesto García-Alfonso,[1] Manuel Barranco,[1,2,3] David A. Bonhommeau,[4] Nadine Halberstadt,[1] Martí Pi,[2,3] and Florent Calvo[5,a)]

AFFILIATIONS

[1] Laboratoire Collisions, Agrégats, Réactivité (LCAR), Université de Toulouse, CNRS, 31062 Toulouse, France
[2] Department FQA, Facultat de Física, Universitat de Barcelona, Diagonal 645, 08028 Barcelona, Spain
[3] Institute of Nanoscience and Nanotechnology (IN2UB), Universitat de Barcelona, Barcelona, Spain
[4] Université de Reims Champagne Ardenne, CNRS, GSMA UMR 7331, 51100 Reims, France
[5] Université Grenoble Alpes, CNRS, LIPHY, F38000 Grenoble, France

[a)] **Author to whom correspondence should be addressed:** florent.calvo@univ-grenoble-alpes.fr

ABSTRACT

The clustering, collision, and relaxation dynamics of pristine and doped helium nanodroplets is theoretically investigated in cases of pickup and clustering of heliophilic argon, collision of heliophobic cesium atoms, and coalescence of two droplets brought into contact by their mutual long-range van der Waals interaction. Three approaches are used and compared with each other. The He time-dependent density functional theory method considers the droplet as a continuous medium and accounts for its superfluid character. The ring-polymer molecular dynamics method uses a path-integral description of nuclear motion and incorporates zero-point delocalization while bosonic exchange effects are ignored. Finally, the zero-point averaged dynamics approach is a mixed quantum–classical method in which quantum delocalization is described by attaching a frozen wavefunction to each He atom, equivalent to classical dynamics with effective interaction potentials. All three methods predict that the growth of argon clusters is significantly hindered by the helium host droplet due to the impeding shell structure around the dopants and kinematic effects freezing the growing cluster in metastable configurations. The effects of superfluidity are qualitatively manifested by different collision dynamics of the heliophilic atom at high velocities, as well as quadrupole oscillations that are not seen with particle-based methods, for droplets experiencing a collision with cesium atoms or merging with each other.

I. INTRODUCTION

Helium-4 clusters at their usual experimental temperatures ($T \sim 0.37$ K)[1] can be considered as superfluid nanodroplets. As such, they have a negligible viscosity and a large thermal conductivity and readily capture any atom or molecule.[2]

The extremely weak interactions of helium with most atomic or molecular dopants make helium nanodroplets (HNDs) particularly suitable for spectroscopic studies.[3–6] The properties of atomic and molecular clusters in ^{4}He droplets have been reviewed by several groups.[1,7–9]

The pickup process used to incorporate the dopant into HNDs is determined by their size and by the conditions in the doping chamber itself. In particular, more than a single dopant per droplet can be incorporated by varying the vapor pressure.[1] The impurities can then move inside the droplet, eventually meeting each other to form clusters or complexes. Such clustering mechanisms are favored by the negligible viscosity and the small volume of the droplet, which facilitates impurity encounters and also by the large thermal conductivity that helps dissipate the energy released by the clustering process.

Clusters formed in ^{4}He droplets do not always show the same structure as in vacuum.[1,10,11] Such differences can be explained by a number of factors. In the pioneering work by Nauta and Miller,[10] long-range dipole–dipole interactions were invoked to interpret the self-assembly between HCN molecules into linear chains.

More generally, the kinetics is expected to play an important role in the clustering process, especially in the common case of sequential pickup. This is because the complexes formed early might be stuck into metastable conformations, rearrangement and isomerization under cryogenic conditions being particularly slow.[12–16] When multiple pickup chambers are used, this can lead to peculiar structures, such as core–shell clusters[17,18] and nanowires.[19] Another interference of helium with the clustering process has been evidenced in the formation of loosely bound "bubble foam" or "quantum gel" structures for light, weakly attractive impurities, such as Ne[20] or Mg.[21,22] This was attributed to the formation of a helium shell around the foreign atoms, preventing the formation of a direct bond between them. In addition, the presence of quantized vortices may further influence the cluster morphology, as vortex cores act as nucleation sites and impurities have a tendency to coalesce, forming filaments along them.[23–25]

Systematic experimental studies on helium clusters and their collision with foreign atoms started in the 1980s,[26,27] as reviewed by Toennies.[28] The first theoretical study of elastic and inelastic scattering of ^{4}He atoms impinging on He clusters was presented by Eichenauer *et al.*, who used a liquid drop plus optical model approach.[29] Depending on the collision parameters and the strength of the dopant–helium interaction, a dopant colliding with a droplet was found to be captured, to escape the droplet, or to go right through it. Upon capture, a significant proportion of the impurity kinetic energy is dissipated into the droplet which relaxes through multiple evaporations of He atoms.[30–32] In addition to the capture of foreign atoms, several groups have recently investigated the soft-landing of helium droplets doped with simple atoms and clusters onto surfaces either experimentally[33] or by means of modeling.[34–36]

Various efficient methods are available to account for quantum nuclear effects at equilibrium, ranging from vibrational configuration interaction,[37] vibrational self-consistent field,[38] Gaussian wavepackets,[39,40] to a broad array of quantum Monte Carlo methods. However, insight into cluster formation and the competition between thermalization and kinetics requires dedicated computational modeling that takes into account the specific nature of the dopants and their interaction with the droplets, in real time. For HNDs that may contain millions of atoms, solving the dynamical problem of capture and subsequent relaxation while accounting for the quantum mechanical nature of ^{4}He happens to be a prohibitive task.

In the present article, we have explored three complementary approaches to address the above issues in real time based on different treatments of the helium droplets. Each approach has been successfully used to simulate different processes occurring in helium nanodroplets. They are compared here, for the first time, on the simulation of the same processes. The time-dependent density functional theory (TDDFT) method, thoroughly described in Refs. 41 and 42, is based on the work by Dalfovo and co-workers.[43] TDDFT and its static version (DFT) treat the ensemble of ^{4}He atoms in an irrotational fluid-like approach at zero temperature, incorporating the peculiarities of the elementary excitation spectrum of ^{4}He that makes it superfluid and including an extra term to account for solid–liquid coexistence.[44] It has recently been applied to the capture and clustering of rare-gas and alkali atoms by He droplets.[31,32,45–49]

A second approach that is suitable for real-time dynamical studies is the ring-polymer molecular dynamics (RPMD) method introduced by Craig and Manolopoulous.[50] It relies on the path-integral framework and provides a description at the atomistic level of details at low but finite temperature, although exchange effects between bosonic ^{4}He atoms are not included. The RPMD method has already been employed to address chemical reactions in helium droplets,[51] including metastable dimerization.[52]

Another atomistic method used here is that of zero-point averaged dynamics (ZPAD), based on the frozen Gaussian wavepacket approach by Heller[53] and the equivalent effective potentials by Sterling *et al.*,[54] which has been successfully used in the dynamical study of rare-gas cluster dissociative ionization inside HNDs.[55–57] The ZPAD approach associates a frozen wavefunction to each He atom, therefore, incorporating zero-point delocalization effects. As in RPMD, exchange effects are ignored, but the method is computationally attractive because the system dynamics can then be treated as classical at the actual HND temperature of 0.4 K, through the use of effective interaction potentials.

Three different physical situations were covered in our exploration of dynamics and relaxation effects in HNDs. Firstly, impurity clustering was chosen owing to its current experimental interest,[8] taking here Ar atoms as the model impurities. The argon atom is heliophilic and resides in the bulk of the droplet, being prone to clusterization from successive pickups. In a recent work by some of us employing the TDDFT approach,[32] the simultaneous collision of different argon impurities was considered and found to produce loosely bound clusters, but the particular choice of highly symmetric initial conditions in these simulations could have affected the results. Here, we have considered the more realistic case of successive pickup, in which argon atoms collide with helium droplets doped with pre-existing argon monomers or small clusters, and investigated the quantitative influence of the collision conditions, as well as the qualitative roles of the possibly preexisting dopant.

Secondly, the capture of Cs atoms, which are barely bound to the He droplet as their binding energy is only about 10 K,[45] provides another challenge to theory. Unlike argon, cesium is heliophobic and tends to reside at the droplet surface, unless it is under the form of a larger cluster.[58–61] In the present work, the collision of a single Cs atom onto a pristine helium droplet was addressed using the three complementary TDDFT, RPMD, and ZPAD approaches, and the effect of collision conditions was assessed.

Finally, we also considered the case of two equivalent droplets merging after being brought into contact. Such a situation has also been already addressed separately earlier by means of TDDFT, both when the two droplets host superfluid vortices[62] and when they do not.[63] Here, the relaxation is caused by the mutual van der Waals attraction between the droplets, in their path toward eventually forming a single double-sized droplet. The droplet-like behavior is highlighted in the merging process, which, thus, constitutes another stringent test on the methodology.

To keep the workload reasonable while still allowing some statistical perspective on the robustness of the results, we have kept the size of the helium droplet to 1000 atoms in our simulations, or two He_{500} droplets experiencing merging. The much larger masses of the argon and cesium atoms relative to helium also justify the usual approximation that their dynamics be considered as classical, only leaving helium atoms to be treated quantum mechanically.

The article is organized as follows: In Sec. II, we outline the three methods used in this work, namely, TDDFT, RPMD, and

ZPAD, in such a way as to provide sufficient insight for the reader who might not be familiar with all of them. In Sec. III, we discuss the results obtained with the three dynamical methods, and some concluding remarks close this paper in Sec. IV. In addition to the main discussion, we provide in the supplementary material a selection of illustrative real-time dynamics of some clustering or relaxation processes inferred from the three computational approaches, as well as some technical details regarding the effective ZPAD potentials.

II. METHODS

The TDDFT,[41,42,64] RPMD,[50,61,65,66] and ZPAD[55–57] methods applied here to helium nanodroplets have been thoroughly described elsewhere. Hence, we limit our description to their essential features and only describe the few new refinements or the features specific to the present systems in more detail.

In each case, we distinguish the methodology at equilibrium, needed to prepare the systems at time $t = 0$, and the methodology needed to address the real-time dynamics following an excitation corresponding to the collision of an impinging argon or cesium atom, or to the sudden contact between two pre-equilibrated droplets.

A. ^{4}He-DFT and TDDFT for liquid helium

Density -functional theory for liquid helium is a phenomenological approach constituting a compromise between accuracy and feasibility for realistic size droplets. The parameters of the functional have been adjusted to reproduce various properties of the bulk superfluid liquid, such as equilibrium density, energy per atom, compressibility, as well as the entire dispersion relation of the elementary excitations.

Since their original introduction by Stringari and co-workers (see, e.g., Ref. 67), functionals have been systematically improved and notably now account for the finite range of interatomic interactions.[43,44] Within He-DFT, the helium droplet is described as a continuous medium at zero temperature. The energy of a N-atom droplet is then written as a functional of the ^{4}He atom density $\rho(\mathbf{r})$ as

$$E[\Psi] = \int d\mathbf{r}\, \frac{\hbar^2}{2m_{\mathrm{He}}} |\nabla\Psi|^2 + \int d\mathbf{r}\, \mathcal{E}_c(\rho), \tag{1}$$

where $\Psi(\mathbf{r})$ is the effective wavefunction (or order parameter) of the superfluid such that $\rho(\mathbf{r}) = |\Psi(\mathbf{r})|^2$ with $\int d\mathbf{r}\, |\Psi(\mathbf{r})|^2 = N$, and the functional $\mathcal{E}_c(\rho)$[44] contains the interaction term within the Hartree approximation and additional terms describing nonlocal correlation effects.[42]

If the droplet carries n atomic impurities A (here, argon or cesium atoms), their effects are taken into account by adding to $E[\Psi]$ in Eq. (1) an external potential under the form $\int d\mathbf{r}\, \mathcal{V}(\mathbf{r})\, \rho(\mathbf{r})$, where $\mathcal{V}(\mathbf{r})$ is the interaction of one single He atom with the cluster calculated by summing He–A interaction potentials as follows:

$$\mathcal{V}(\mathbf{r}) = \sum_{i=1}^{n} V_{\mathrm{He-A}}(|\mathbf{r} - \mathbf{r}_i|), \tag{2}$$

with $\mathbf{r}_i$ being the position of the ith A atom.

The droplet equilibrium configuration is obtained by solving the Euler–Lagrange equation,

$$\left\{ -\frac{\hbar^2}{2m_{\mathrm{He}}}\nabla^2 + \frac{\delta\mathcal{E}_c}{\delta\rho} + \mathcal{V}(\mathbf{r}) \right\} \Psi = \mu\Psi, \tag{3}$$

where μ is the ^{4}He chemical potential corresponding to the number of He atoms in the droplet.

Equation (3) is solved in Cartesian coordinates using a space-step of 0.35 Å in the presence of Ar atoms, 0.4 Å in the presence of a Cs atom, and 0.44 Å for merging He_{500} droplets. In the case of argon clusters, their configuration is kept fixed at the gas phase structure,[68] since the presence of helium is not expected to introduce any significant change to the structure of the preformed argon cluster[32,69,70] due to the much weaker He–Ar interaction compared to Ar–Ar.[71]

The time evolution equations for the effective wavefunction $\Psi(\mathbf{r})$ and impurity positions $\mathbf{r}_i$ are obtained by minimizing the action,[32] which yields

$$i\hbar\frac{\partial}{\partial t}\Psi(\mathbf{r}) = \left[-\frac{\hbar^2}{2m_{\mathrm{He}}}\nabla^2 + \frac{\delta\mathcal{E}_c}{\delta\rho(\mathbf{r})} + \sum_{i=1}^{n} V_{\mathrm{He-A}}(|\mathbf{r} - \mathbf{r}_i|) \right] \Psi(\mathbf{r}), \tag{4}$$

$$m_{\mathrm{A}}\ddot{\mathbf{r}}_i = -\left\{ \int d\mathbf{r}\, V_{\mathrm{He-A}}(|\mathbf{r} - \mathbf{r}_i|) \nabla\rho(\mathbf{r}) + \sum_{i\neq j} \left[\frac{\mathbf{r}_i - \mathbf{r}_j}{r_{ij}} \frac{dV_{\mathrm{A-A}}}{dr}(r)\Big|_{r=r_{ij}} \right] \right\} \quad (i = 1, \ldots, n), \tag{5}$$

where the last term in Eq. (5) is only present for clusters, $r_{ij} = |\mathbf{r}_i - \mathbf{r}_j|$, and the time dependence of the variables has been omitted for clarity.

In order to solve Eqs. (4) and (5), initial values for the $\{\mathbf{r}_i, \dot{\mathbf{r}}_i\}$ variables and the effective wavefunction $\Psi(\mathbf{r})$ have to be specified. When simulating Ar_n clustering, they were taken as the He effective wavefunction and the Ar atom positions $\{\mathbf{r}_i(0)\}, i = 1, \ldots, n-1$ obtained as the equilibrium configuration of the preformed solvated (n-1)-atom cluster by solving Eq. (3), with $\{\dot{\mathbf{r}}_i(0)\} = 0$. When simulating Cs collisions or droplet merging, the He effective wavefunction was taken as that of the pure He_{1000} or He_{500} droplets, respectively. The values of the remaining variables, $\{\mathbf{r}_n(0), \dot{\mathbf{r}}_n(0)\}$, were chosen to yield the desired impact parameter and kinetic energy of the impinging impurity.

The He–Ar and He–Cs interaction potentials were taken from Tang and Toennies (TT),[71] and from Patil,[72] respectively. Equations (3)–(5) were solved using the ^{4}He-DFT BCN-TLS computing package.[73] In particular, Cartesian coordinates were used and a fast Fourier transform[74] was employed to evaluate the convolution integrals entering the DFT mean-field definition.

The time-dependent equations (4) and (5) were numerically solved using a Hamming predictor–modifier–corrector initiated by a fourth-order Runge–Kutta–Gill algorithm,[75] with time steps of 0.1 and 0.5 fs in the presence of argon and cesium atoms, respectively, and 1 fs for the merging problem. When needed, absorbing boundary conditions were implemented to prevent evaporated helium atoms from reentering the simulation box (periodic boundary conditions are imposed to use the fast Fourier transform). During the integration of the time evolution equations, the positions of all impurities were free to relax. Reference 64 and references therein

provide more details on how the DFT and TDDFT equations are solved in practice.

B. The RPMD approach

RPMD is an approximate method for solving the time-dependent quantum dynamics problem based on the path-integral formalism, which is exact in the short time and harmonic limits.[50] Its connections with semiclassical instanton theory[76] and also with centroid molecular dynamics and Matsubara dynamics have been thoroughly explored by Hele and co-workers.[77] In the context of real-time dynamics at thermal equilibrium, RPMD has been used to compute vibrational spectra in anharmonic systems[78–80] to determine transport properties in condensed systems[81,82] and also to characterize reactive collisions dynamics.[83,84] The method was also used occasionally to explore various out-of-equilibrium situations induced by a vertical excitation or some momentum impulse[85,86] and was shown also in this context to be exact in the limit of short times, harmonic potentials, or high temperatures.[87]

Briefly, the method relies on the Feynman formalism of imaginary time path integrals and assimilates the quantum dynamics of the many-body system to an effective classical dynamics of a higher-dimensional system, each particle being described by a ring-polymer of P monomers or beads. In practice, with $\{\mathbf{R}_\alpha, \alpha = 1, \ldots, P\}$ denoting the set of positions of these monomers, the dynamics is Hamiltonian and ruled by the effective potential

$$V_{\text{eff}}(\{\mathbf{R}_\alpha\}) = \frac{1}{P}\sum_{\alpha=1}^{P} V(\mathbf{R}_\alpha) + \sum_{\alpha=1}^{P}\sum_{i\in\text{atoms}} \frac{m_i P}{2\beta^2\hbar^2}\|\mathbf{r}_{\alpha,i} - \mathbf{r}_{\alpha,i+1}\|^2, \quad (6)$$

where $\beta = 1/k_B T$ with k_B and $\hbar$ being the Boltzmann and reduced Planck constants, respectively, and T being the temperature. In Eq. (6), $\mathbf{r}_{\alpha,i}$ denotes the position of particle i of replica α with the cyclic condition $\mathbf{r}_{P+1,i} = \mathbf{r}_{1,i}$, the entire set of positions for replica α being referred to as $\mathbf{R}_\alpha$. In conventional (thermostated) path-integral molecular dynamics (PIMD), each particle with position $\mathbf{r}_{\alpha,i}$ is associated with a momentum $\mathbf{p}_{\alpha,i}$ and a mass $m_{\alpha,i}$ that can be freely adjusted in order to improve sampling efficiency. Within RPMD, the masses are not arbitrary but all set to the physical values, $m_{\alpha,i} = m_i$ for all $\alpha = 1, \ldots, P$.

In practice, all variables are transformed into normal modes in order to decouple the harmonic part of the Hamiltonian, which in turn enables the use of the reference system propagation algorithm (RESPA)[88] to accelerate the integration of the trajectory. The initial conditions of RPMD trajectories need to be properly equilibrated, and each particle was coupled to an individual Nosé–Hoover variable, within conventional PIMD trajectories. Such massive thermostating was used to prepare samples of phase space configurations for the various systems under study, namely, pure helium droplets containing 500 or 1000 atoms and, in the latter case, possibly doped with either one atom, one dimer, or one tetramer of argon.

A ring contraction technique[89] was also employed to reduce the number of beads needed to describe the heavier atoms. A temperature of $T = 1$ K and a Trotter number of $P = 256$ were chosen to describe the helium atoms, with $P = 16$ beads for argon and cesium atoms. Such a moderately high temperature was necessary to perform PIMD and RPMD simulations within a reasonable amount of computing time while maintaining a good precision: The binding energy obtained for pure He_{1000} droplets with 256 beads is in reasonable agreement with reference results.

Efficient Lennard-Jones versions of the TT potential[71] were employed to describe interactions between the rare gases, with corresponding parameters $\varepsilon_{\text{He–He}} = 10.76$ K, $\varepsilon_{\text{Ar–Ar}} = 143.4$ K, $\varepsilon_{\text{He–Ar}} = 29.61$ K, $\sigma_{\text{He–He}} = 2.635$ Å, $\sigma_{\text{Ar–Ar}} = 3.346$ Å, and $\sigma_{\text{He–Ar}} = 3.115$ Å.

In simulating collisions between argon or cesium projectiles onto pure or doped helium droplets, random phase space configurations were borrowed from the PIMD samples for both the projectile and the target cluster and served as initial conditions. Those configurations were randomly rotated and initial positions for the centroid of the projectile were imposed so that the centers of mass between the collision partners are separated initially by 50 Å along the x-axis and by an impact parameter $b = 0$ or $b = 10$ Å along the y-axis. The thermostated PIMD trajectories used for sampling initial conditions used a time step of 0.1 fs, while a longer time step of 0.5 fs could be employed to propagate the RPMD trajectories owing to the RESPA trick. The overall computational load of RPMD trajectories is approximately P times that of classical molecular dynamics.

C. The ZPAD approach

ZPAD is a mixed quantum-classical method designed to model the dynamics of dopants embedded in a quantum environment. It provides an approximate description of the quantum delocalization of helium atoms at almost the same computational cost as classical dynamics. The method originates from the work of Sterling *et al.*[54] who modeled the dynamics of pure and Li-doped solid parahydrogen by representing H_2 as Gaussian particles. As a result, the H_2 dynamics was similar to the frozen Gaussian approach of Heller[53] and can be described as classical dynamics using effective interaction potentials. Slavíček *et al.* later applied this idea to simulate the photodissociation of hydrogen halides in floppy neon clusters.[90] These authors implemented an iterative procedure to determine neon wavefunctions and were able to rapidly converge accurate effective Ne–Ne potentials. ZPAD, as used in the present work, was introduced as a direct extension of Ref. 90 to the fragmentation dynamics of neon- and argon-doped helium clusters[55–57,91] by solving the convergence problem due to the extensive delocalization of the helium atom wavefunction.

The ZPAD method relies on the iterative determination of the frozen wavefunction describing the quantum delocalization of the He atoms and of the inferred effective He–He pair potential. The iterative procedure is detailed in Refs. 55–57 and 91; hence, only its essential features are recalled here. At each iteration, a classical simulation of the He_N system at the experimentally relevant temperature of $T = 0.38$ K is performed using the current, iteratively determined He–He pair potential (i.e., the classical He–He potential at the first iteration and an effective, but nonconverged, He–He potential at later iterations). The next He wavefunction is obtained by solving the radial Schrödinger equation for a helium atom in the average environment of the remaining He atoms, assumed to be spherical, using the current effective potential convoluted with the pair distribution function. The classical potential is then doubly convoluted with the squared modulus new He wavefunction to obtain the new effective potential, and the process is repeated until convergence. The final

effective potential is characterized by a much shallower well and a larger equilibrium distance.

In practice, it was necessary to truncate the He wavefunction at R = 1.6 Å in order to reach convergence.[57] Note that a recent method along the same lines as the ZPAD method does not determine an effective wavefunction for helium atoms but directly the effective potential itself.[92] Here, the effective potential well depth was found to be 1.81 K at an equilibrium distance of 4.39 Å.

Because argon atoms are fully solvated in helium droplets, it is relevant to incorporate delocalization effects in the He–Ar interaction as well and, hence, to design a corresponding effective potential. Neglecting any delocalization effect of the Ar atom, the Tang–Toennies Ar–He interaction potential was convoluted with the squared modulus of the He wavefunction obtained previously. The effective Ar–He potential thus obtained has a binding energy of 13.57 K at an equilibrium distance of 4.17 Å, to be compared with 29.59 K at 3.498 Å for the original potential.[71] Numerical details of the He–He and Ar–He effective potentials used in this study are given in the supplementary material, and the reader is referred to Refs. 55–57 and 91 for more information about the iterative procedure employed to converge the He–He effective potential. In contrast to argon, heliophobic cesium atoms were treated fully classically in their interaction with helium.

The zero-point averaged dynamics of the doped HND is then carried out by performing classical dynamics for the He and the dopant atoms using as total potential energy the sum of effective He–He interactions, dopant–dopant interactions, and He–dopant interactions (effective for Ar and classical for Cs). All ZPAD trajectories employed a time step of 1 fs.

III. RESULTS

Before addressing the time-dependent processes involving heliophilic or heliophobic impurities or the natural relaxation of droplets merging, and since we need them as initial conditions, it is necessary to consider the equilibrium case of helium nanodroplets themselves. Figure 1(a) shows the radial densities of helium atoms in the He_{1000} droplet determined with respect to the droplet center of mass, as predicted by density -functional theory, path-integral MD at equilibrium, and zero-point averaged MD method at 0, 1, and 0.38 K, respectively. Likewise, Fig. 1(b) depicts the He–Ar radial distributions for He_{1000} droplets doped with a single argon atom lying inside. Overall, the helium density obtained for the pristine helium droplet is extremely smooth with the DFT approach. Such a smooth radial profile is consistent with earlier results, including diffusion Monte Carlo (DMC) simulations.[42] Within the PIMD description, some minor shell structuration can be perceived, which becomes even more clear with ZPAD. This behavior is a signature of the mostly classical character of ZPAD. In particular, the density at a vanishing distance from the center of mass is extremely small and about 500 times smaller than the first peak at 2.5 Å, which indicates rigidity near the droplet center, vacant from any atom. Note, however, that the average density profile is reasonable, especially compared to the one obtained from the original He–He potential (not shown).

In the presence of the argon impurity, the helium atoms preferentially localize around it at a distance close to 4 Å and the three

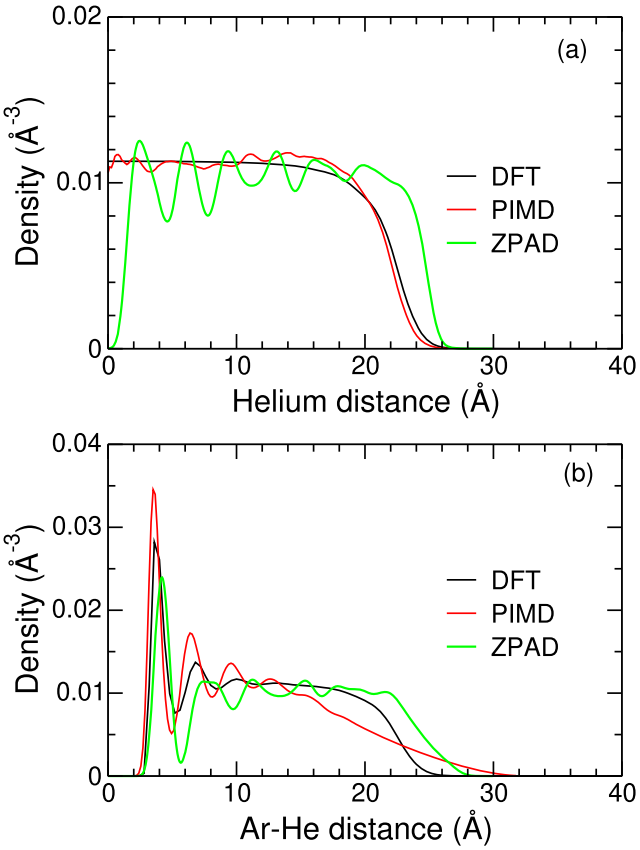

FIG. 1. Equilibrium density profiles of the He_{1000} and $ArHe_{1000}$ droplets obtained with the DFT, PIMD, and ZPAD methods. (a) Pure helium droplets. (b) Droplets doped with a single argon atom.

methods concur in predicting even a second shell, although much less localized than the first one. For such problems of a central heliophilic impurity, DFT was also shown to be robust against DMC calculations.[93,94] The average radius of the first solvation shell is slightly larger with the ZPAD method and slightly smaller with the RPMD method by a fraction of angström. Interestingly, the decay of the He–Ar radial distribution is much smoother with the PIMD method at equilibrium. Inspection of configurations reveals that this is caused by the argon impurity being rather mobile inside the droplet, exploring a sphere of radius of about 5 Å around the droplet center. Such a radius is consistent with the extra broadening of the distribution exhibited by the PIMD approach and could also be partly due to the higher temperature of 1 K used with this method. The ZPAD method follows the behavior obtained with DFT, albeit with a first shell that is more marked and a more extended droplet. Thus, in the presence of a very attractive dopant, the more rigid behavior of the ZPAD method makes a smaller difference with the DFT results since the droplet itself is somewhat structured by the dopant.

Besides structural properties, the methods can also be compared with each other on an energetic footing. The binding (virial) energy of the He_{1000} droplet is found to be about −6212 K with

RPMD, or about 20% higher in magnitude than the DFT value (−5396 K), as obtained with the functional of Ref. 44. The corresponding value predicted by the ZPAD method amounts to −9600 K, and it is consistent with the overstructuration of the droplet relative to the DFT reference calculation. This is also the case for RPMD, although to a lesser extent.

A solvation energy E_{solv} of the single argon impurity can also be evaluated from the difference between the total energies of the $ArHe_{1000}$ and pristine He_{1000} systems. With the DFT method, we find $E_{solv}(Ar) = 5598 - 5396 = 202$ K, or about seven times the Ar–He well depth at equilibrium. This value is twice as large as that found with the ZPAD method [$E_{solv}(Ar) = 9716 - 9615 = 101$ K] and 67% smaller than that found with the PIMD method [$E_{solv}(Ar) = 6549 - 6212 = 337$ K]. The apparent underestimation of Ar solvation energy in ZPAD calculations is related to the use of an effective Ar–He potential whose well depth is 2.2 times smaller than that of the Tang–Toennies Ar–He interaction potential (see Fig. 1 in the supplementary material). However, the ZPAD solvation energy is equal to 7.4 times the minimum energy of the effective Ar–He interaction, which is also close to the ratio found in the He-DFT simulation.

A. Heliophilic Ar atoms

In order to evaluate the ability of the three methods to describe the capture and coagulation of Ar atoms, as well as to shed more light on the clustering process inside helium droplets, several simulations were carried out in which an argon atom is projected at fixed velocity onto a He_{1000} droplet doped with a single argon atom or a small Ar_n cluster with $n = 2$ or 4, both being taken in their gas phase equilibrium geometry (regular tetrahedron for the tetramer). In typical experimental conditions (nozzle diameter of 5 μm and temperature of 24 K, He pressure of 80 bars), the He droplets' velocity is ~480 m/s.[95] In a pickup cell at 370 K (temperature mentioned by Theisen *et al.*[96]), Cs has an average velocity of 260 m/s randomly oriented with respect to that of the He beam. This yields a range of relative He droplet–Cs velocities between 220 and 740 m/s. The same argument applied to Ar at room temperature (300 K) gives an average Ar velocity of 430 m/s and a range of relative Ar-droplet velocity of 50–910 m/s. Here, we selected velocities of 500 and 1000 m/s for argon projectiles and velocities of 50 and 500 m/s for cesium projectiles. Two different impact parameters were also tested: $b = 0$ or 10 Å.

The various possible products of the trajectories are depicted in Fig. 2. We first discuss the possible formation of an Ar dimer upon the Ar + $ArHe_{1000}$ collision to introduce the main features of the dynamics. Even at thermal velocities of 500 m/s, the capture of impurities such as Ar atoms by weakly bound He droplets appears to be a rather violent process, as particularly illustrated by recent TDDFT simulations.[32,47] It was notably shown that a sizable fraction of the collision energy of the impinging dopant is transferred to the droplet during the first stages of the collision, producing shock waves and nucleating quantized vortices.[32,47,48] As a result, a few picoseconds after the projectile enters the droplet, its velocity drops below the Landau critical velocity, which is about 118 m/s for the functional considered here.[42] At the same time, a high density helium structure builds around the incoming projectile, which, together with the helium solvation shell around the embedded cluster, can hinder the formation of a direct Ar–Ar bond. However, the remaining kinetic energy of the projectile may be sufficient to enable the formation of a bound cluster with the host atoms inside the droplet. This situation occasionally takes place in our simulations, as illustrated in Fig. 2. However, the propensity for forming Ar–Ar bonds not only depends on the available collision energy but also on the impact parameter, high values of b being necessarily associated with some rotational energy and a concomitantly lower relative translational energy available for breaking the solvation shells and leading to coagulation. At 500 m/s, and within the TDDFT framework, Ar_2 is, thus, formed if the collision takes place at $b = 0$ but not at $b = 10$ Å. This less favorable clustering, also found in the case of Ne,[49] can be interpreted as the trapping of a significant proportion of the collision energy

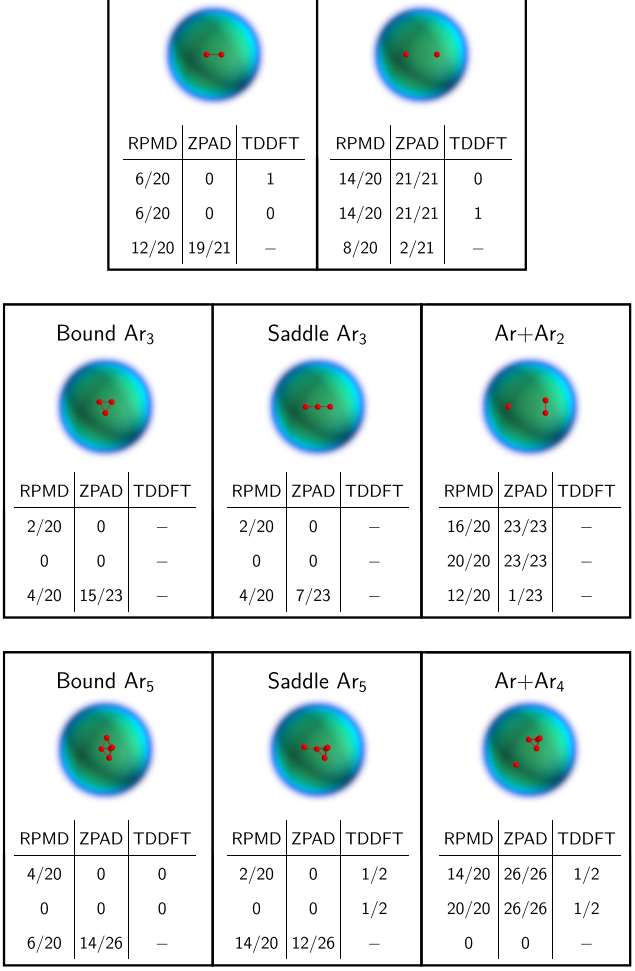

Bound Ar_2			Ar+Ar		
RPMD	ZPAD	TDDFT	RPMD	ZPAD	TDDFT
6/20	0	1	14/20	21/21	0
6/20	0	0	14/20	21/21	1
12/20	19/21	–	8/20	2/21	–

Bound Ar_3			Saddle Ar_3			Ar+Ar_2		
RPMD	ZPAD	TDDFT	RPMD	ZPAD	TDDFT	RPMD	ZPAD	TDDFT
2/20	0	–	2/20	0	–	16/20	23/23	–
0	0	–	0	0	–	20/20	23/23	–
4/20	15/23	–	4/20	7/23	–	12/20	1/23	–

Bound Ar_5			Saddle Ar_5			Ar+Ar_4		
RPMD	ZPAD	TDDFT	RPMD	ZPAD	TDDFT	RPMD	ZPAD	TDDFT
4/20	0	0	2/20	0	1/2	14/20	26/26	1/2
0	0	0	0	0	1/2	20/20	26/26	1/2
6/20	14/26	–	14/20	12/26	–	0	0	–

FIG. 2. Diversity of products obtained upon collisions between an impinging argon atom and He_{1000} droplets doped with an argon monomer, a dimer, or a tetramer, and occurrence statistics of these products for various impact parameters b and collision velocities v. For each of the RPMD, ZPAD, and TDDFT methods, and from top to bottom, the statistics given correspond to collisions at $b = 0$ and $v = 500$ m/s; $b = 10$ Å and $v = 500$ m/s; $b = 0$ and $v = 1000$ m/s, respectively.

into orbital rotation, which makes it difficult to transfer it to relative translation, the only available mechanisms being vortex nucleation and the appearance of surface capillary waves.[31,97,98]

The cases studied within the RPMD and ZPAD approaches included $b = 0$ and 10 Å for $v = 500$ m/s and $b = 0$ for $v = 1000$ m/s. The latter case was not addressed with TDDFT as it would imply a prohibitively short time step to keep the total energy of the system constant. Within the RPMD approach, 20 independent trajectories were performed for each set of b and v values. Ar_2 is found to be formed in about one-third of the cases, no significant effect of the impact parameter being noticeable. At the much higher collision energy brought by the projectile impinging on the droplet at 1000 m/s, Ar_2 is formed twice as easily. With the ZPAD method, the situation is contrasted, no dimer being produced at 500 m/s but, conversely, most trajectories at 1000 m/s leading to stable Ar_2 products.

We now turn to the coagulation of impinging Ar atoms on a He droplet containing a preformed Ar cluster. RPMD and ZPAD collision simulations were carried out for helium droplets doped with an argon dimer prepared at its equilibrium geometry. As was the case with $ArHe_{1000}$, and with both methodologies, it is quite difficult to form the expected trimer in its stable geometry (equilateral triangle, denoted as "Bound" in Fig. 2) with an argon atom impinging at 500 m/s. Such a successful coagulation occurs at $b = 0$ in RPMD calculations with 10% probability at 500 m/s and 20% probability at 1000 m/s. With ZPAD, trimers are formed only at the higher collision velocity but with about 65% probability. However, intermediate situations occasionally take place with a cluster having fewer Ar–Ar bonds being formed and occupying higher-order configurations on the potential energy surface instead of the only true minimum, usually close to the linear saddle point. This situation is denoted as "Saddle" in Fig. 2. In the present case, nearly linear trimers are obtained with 20%–35% probability at 1000 m/s velocity depending on the method, with two such events among 20 trajectories also occurring at 500 m/s and $b = 0$ with RPMD. In the remaining cases, the Ar projectile and the preformed dimer are still roaming inside the droplet at the end of the simulations. They could eventually meet and form a loosely bound trimer, analogous to the loose Ar_6 structure found in Ref. 32, but their low kinetic energy makes it improbable that they could form a trimer in the gas phase configuration.

The three frameworks of TDDFT, RPMD, and ZPAD were used to address the case of Ar projectiles impinging on Ar_4 embedded in He_{1000}, under the same collision conditions as used for the previous systems. Here, again the expected product Ar_5 only has one minimum which is a face-sharing double tetrahedron, although it has a greater diversity of stationary points than Ar_3. At 500 m/s, and for both $b = 0$ and $b = 10$ Å, two simulations were performed using TDDFT, with the argon atom approaching the target cluster toward an apex atom or oppositely toward a facet. The four resulting simulations lead to the formation of a higher-energy, non-minimum configuration in half of the cases, with the incoming argon binding to two argons from an edge of the tetramer, the other half being associated with unconnected products. With the RPMD approach, low collision velocities usually do not produce larger clusters, but the stable pentamer is obtained in 20% of the cases and higher-order configurations in 10% of the cases, provided that $b = 0$. Such configurations are still denoted as "saddle" in Fig. 2, although no specific attempt was made to characterize the order of the corresponding stationary points. Raising the collision velocity to 1000 m/s always produces connected pentamers, but mostly (2/3) as higher-energy configurations. The ZPAD model is qualitatively consistent with the RPMD description, pentamers being only produced in significant amounts when the collision velocity reaches 1000 m/s.

From a more quantitative perspective, Fig. 3 shows the Ar–Ar distance in collisions between Ar and $ArHe_{1000}$ at the three collision

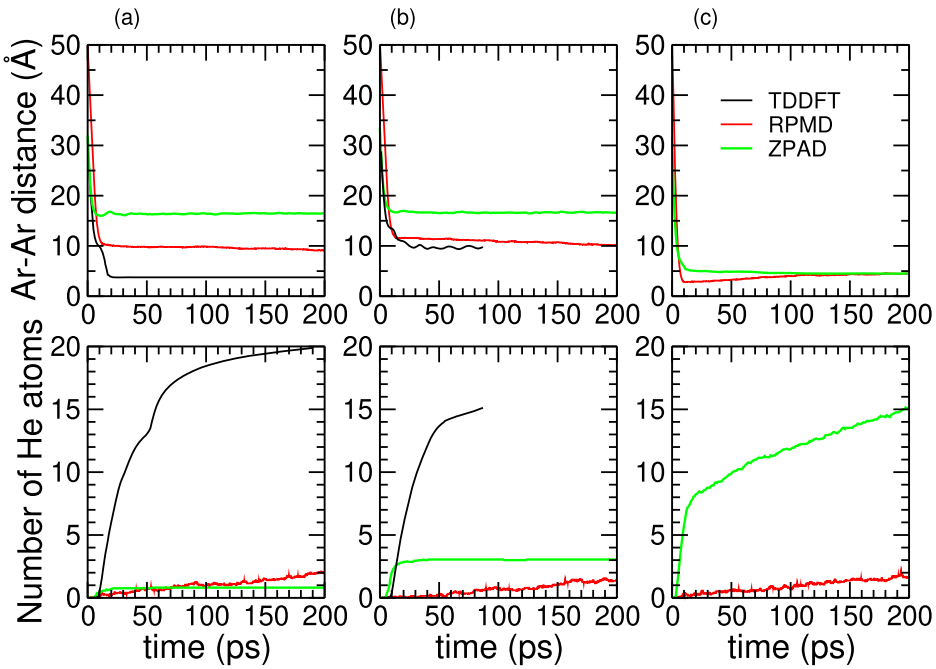

FIG. 3. Ar–Ar distance and number of evaporated helium atoms upon collision of an Ar atom onto $ArHe_{1000}$ droplets, as predicted by the RPMD, ZPAD, and TDDFT methods, at three collision conditions and as a function of time. For RPMD and ZPAD, the results are averaged over 20 and 21 independent trajectories, respectively. (a) $b = 0$ and $v = 500$ m/s; (b) $b = 10$ Å and $v = 500$ m/s; (c) $b = 0$ and $v = 1000$ m/s.

conditions, as predicted by the three methods and possibly averaged over the independent trajectories in the RPMD and ZPAD cases, as a function of time.

At zero impact parameter, and consistent with the statistics reported in Fig. 2, these distances show that the projectile enters the droplet deeper when modeled with the TDDFT method, then RPMD, relative to ZPAD. Increasing the impact parameter or the collision velocity naturally increases or decreases the average distance, respectively. Interestingly, at 1000 m/s, the average Ar–Ar distance reaches a minimum after about 10 ps and slowly increases later on when the dynamics is described with the RPMD method. This behavior is indicative of some recoil motion once the two argon atoms have connected to each other, such a motion being absent with the ZPAD approach. This contrasted behavior is actually related to the more diffuse character of the argon impurity into the He_{1000} droplet seen on the radial distribution of Fig. 1(b), which produces some trajectories where the argon projectile connects with the embedded argon atom quite early during the collision, giving it a partial elastic character with the dimer relaxing to its equilibrium distance over shorter time scales.

The TDDFT description predicts straightforward formation of the Ar dimer under $b = 0$ and 500 m/s collision velocity. On a smaller scale, about ten damped oscillations with a period of about 1.1 ps can be seen,[32] corresponding to vibrational energy dissipation to the droplet. However, only a loose dimer distant by about 10 Å is formed when $b = 10$ Å. The time oscillations with an approximate period of 10 ps seen in the upper panel of Fig. 3(b) indicate some relative motion between the two embedded impurities that is associated with more global deformations of the droplets but not to vibrations of the dimer, as was the case for $b = 0$. This combined motion that preserves the Ar–Ar distance near 10 Å is best seen directly on the animations provided in the supplementary material.

A direct manifestation of the relaxation dynamics following the clusterization process is found in the emission of helium atoms that is expected as the main pathway to release the excess energy brought by the collision. The average numbers of helium atoms released from the He_{1000} droplet as a function of time corresponding to the same TDDFT, RPMD, and ZPAD trajectories are shown in the lower panels of Fig. 3. For this property, the TDDFT method predicts that evaporation takes place very quickly and steadily, a kink near 50 ps being indicative of a further ejection of helium matter once the already formed dimer bounces against the droplet surface. The rate of variations of the number of evaporated helium atoms is not linear with TDDFT, and we, thus, expect more atoms to evaporate if the trajectories could be integrated further, and exceed the already significant numbers of 20 or 15 found at $b = 0$ and $b = 10$ Å, respectively. Based on the known energetics of the various processes involved in the dimer formation, we can further predict that about five more helium atoms should evaporate to reach equilibrium again in the TDDFT case. More precisely, at 500 m/s velocity, the energy brought by the collision is about 600 K. The formation of the dimer releases an additional 143.5 K, and the solvation of the projectile atom a further 202 K from the aforementioned data, giving a total of about 950 K to be dissipated. In the present TDDFT simulations, we find that the total energy has decreased by about 765 K after 200 ps, or 80% of this total amount. The remaining 20%, thus, correspond to five atoms that remain to be evaporated.

In contrast, both the RPMD and ZPAD methods significantly underestimate the number of helium atoms emitted by the coagulation process at low collision velocity, between one and three atoms only being evaporated, and this result is a striking manifestation of the different rates at which the energy dissipates in superfluid or non-superfluid systems. Only at 1000 m/s does the ZPAD method predict a copious amount of helium atom evaporations, but still lower in magnitude than what is predicted by TDDFT at 500 m/s only, hence the results reported in the lower panel of Fig. 3(c) are still probably underestimated. At such a higher collision energy, the RPMD method predicts surprisingly robust droplets with a very high propensity for storing the excess energy from the collision and not releasing much of it through evaporative cooling. This points at a possible shortcoming of the path-integral description, which might insufficiently redistribute the excess energy into the intermolecular modes. While the kinetic temperatures inferred from the RPMD trajectories remain very close to the initial imposed value of 1 K, it may well be that the time needed to redistribute the excess energy created by forming the Ar_2 bond into the dissociative mode of an (outer) helium atom is still too long owing to the overstructured nature of the helium droplet within the RPMD model. In addition, inspection of the ZPAD trajectories indicates that several of the helium atoms that are evaporated are actually scattered early during the trajectory after the argon projectile hits the droplet, the slower decay occurring at longer times resulting from the actual bond formation.

One clearly missing ingredient from the RPMD and ZPAD approaches is the role of exchange statistics that is responsible for the superfluid behavior correctly accounted for by the DFT method. Although the superfluid character is expected to favor bond formation due to the low viscosity of the embedding medium, coagulation does not systematically occur either even with the TDDFT approach, and such processes are occasionally found also with the RPMD method in which the helium droplet is treated as a viscous host. The limitations of the ZPAD approach in underestimating the propensity for argon cluster growth can be assigned to the excessive structuration of the liquid, which itself is due to to an excessively deep He–He effective potential. This points to a too short truncation distance used in the convergence of the frozen wavefunction.

B. Heliophobic Cs atoms

Crossed-beam experiments involving Cs atoms and either ^{4}He or ^{3}He droplets were originally conducted by Gspann and Ries several decades ago[27] and subsequently by Lewerenz and co-workers[95] for droplets containing 10^3–10^4 helium atoms. Cesium binds to helium very weakly, by ~10 K only;[45] therefore, hoping to get it captured by spontaneous collisions appears as rather challenging. Earlier TDDFT simulations of Cs impinging onto $^4He_{1000}$ superfluid droplets produced a rich phenomenology.[45] For head-on collisions ($b = 0$), the cesium projectile was found to be captured, to bounce back, or to pierce through the droplet depending on the collision velocity.[45,47] In the present work, additional TDDFT trajectories were carried out at $b = 10$ Å and the two velocities of $v = 50$ and 500 m/s.

The qualitative outcomes of these trajectories, together with the results obtained using the alternative RPMD and ZPAD methods and their associated statistics, are given in Fig. 4.

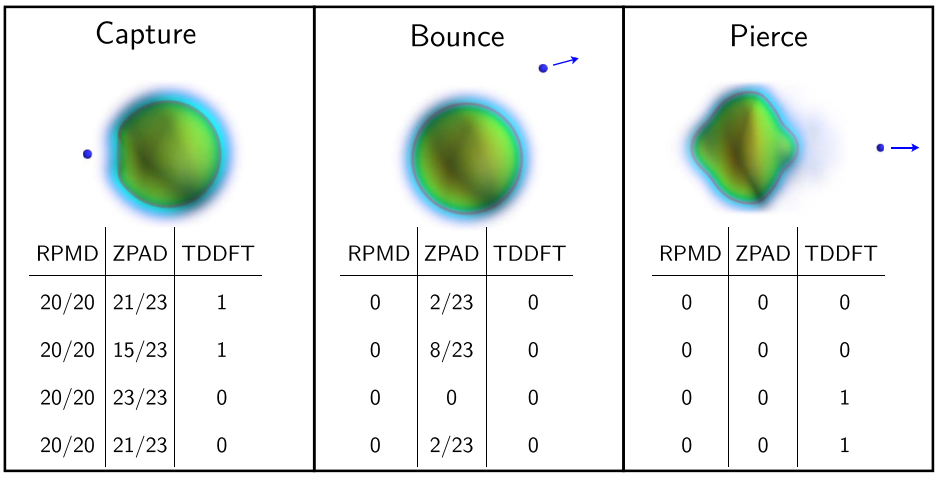

RPMD	ZPAD	TDDFT
20/20	21/23	1
20/20	15/23	1
20/20	23/23	0
20/20	21/23	0

RPMD	ZPAD	TDDFT
0	2/23	0
0	8/23	0
0	0	0
0	2/23	0

RPMD	ZPAD	TDDFT
0	0	0
0	0	0
0	0	1
0	0	1

FIG. 4. Three possible outcomes upon collisions between an impinging cesium atom and He_{1000} droplets, and corresponding occurrence statistics of these products for various impact parameters b and collision velocities v. For each of the RPMD, ZPAD, and TDDFT methods, and from top to bottom, the statistics given correspond to collisions at $b = 0$ and $v = 50$ m/s; $b = 10$ Å and $v = 50$ m/s; $b = 0$ and $v = 500$ m/s; $b = 10$ Å and $v = 500$ m/s, respectively.

At the lowest velocity, all methods find that the alkali projectile eventually gets captured by the droplet in all (RPMD) or most (ZPAD) of the cases, and possibly scattered in 1/3 of the cases when $b = 10$ Å with ZPAD. The capture found with TDDFT with $b = 10$ Å consistently completes the results of Ref. 45 using the same methodology (Cs atom being captured for $b = 9$ Å, scattered for $b = 11$ Å).

Qualitative differences between the three methods are found when the collision takes place at 500 m/s, in which case the projectile remains captured when modeled using RPMD or ZPAD, while it pierces through the droplet within the TDDFT framework.

Figure 5 analyzes in more detail the collision process, by showing the distance between the cesium atom and the center of mass of the helium droplet, as a function of time. As shown in this figure, under the conditions leading to its capture, the Cs projectile starts by entering the droplet by a few angströms before it is eventually pushed back toward the droplet surface and forms a dimple. The penetration depth is about 2 Å with RPMD and ZPAD, but closer to 5 Å with TDDFT, which we explain as due to the much softer nature of the droplet with this method. Another qualitative difference is the orbiting nature of the Cs atom sent toward the droplet with $b > 0$ in TDDFT calculations, whereas the two particle-based methods predict a fast conversion of the rotational energy into internal vibrational modes owing to their description of the helium droplet host as a viscous medium. Such differences are well captured by the movies provided in the supplementary material.

At 500 m/s velocity, the capture of the cesium atom remains the dominant process in ZPAD and RPMD simulations, but the penetration depth is unsurprisingly and significantly larger, even when the impact parameter is taken as 10 Å. However, the TDDFT method predicts that the projectile pierces through the droplet upon head-on collisions, as seen from the distance in Fig. 5(b) reaching the value 0 for $b = 0$. For $b = 10$ Å, this distance reaches a minimum of ~12 Å. Inspection of the corresponding movie reveals that the projectile also pierces the droplet, and the turbulences created in the helium host move it by about 2 Å away from the minimum distance of 10 Å corresponding to the impact parameter value.

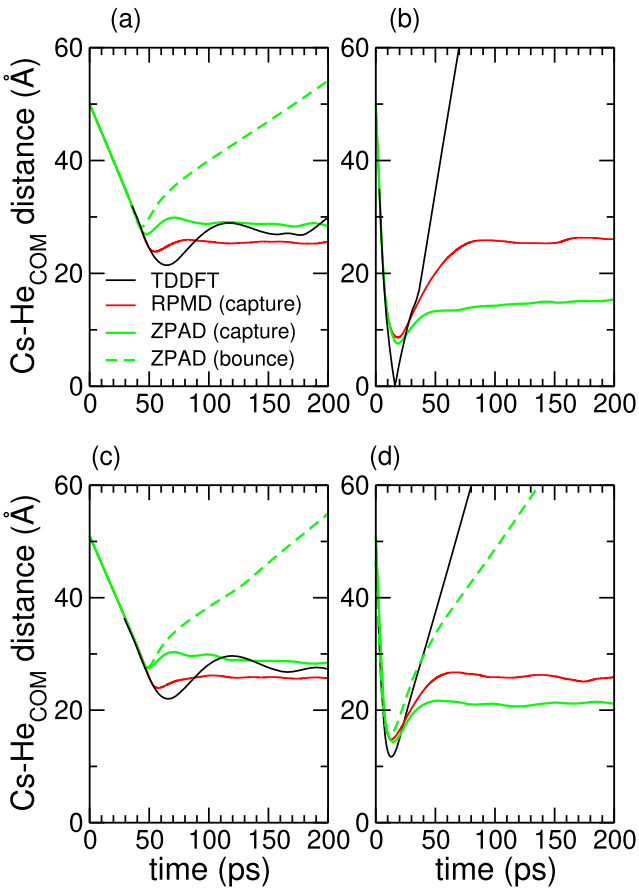

FIG. 5. Average distance between the impinging Cs atom and the center of mass of the He_{1000} droplet as a function of time, as obtained with the RPMD, ZPAD, and TDDFT methods under different collision conditions. The RPMD results are averaged over 20 independent trajectories. The ZPAD results are averaged over subsets of independent trajectories leading to capture or bouncing outcomes. (a) $b = 0$ and $v = 50$ m/s; (b) $b = 0$ and $v = 500$ m/s; (c) $b = 10$ Å and $v = 50$ m/s; (d) $b = 10$ Å and $v = 500$ m/s.

A closer inspection of the TDDFT results for $b = 0$ at 500 m/s collision velocity shows that the velocity of the outgoing Cs atom that has pierced through the droplet approaches the Landau velocity for the functional used in this work. The existence of such a limiting velocity has been observed in a combined experimental and ^{4}He-TDDFT study by Brauer *et al.*[99] for a silver atom ejected through photoexcitation from inside a helium nanodroplet. This effect cannot be reproduced by the other two methods.

In both cases, the droplet experiences a significant deformation, which can be quantified by computing a normalized quadrupole moment Q_{zz}/R_g^2 along the same direction (noted as z) as the collision velocity vector:

$$Q_{zz} = \frac{1}{N}\int \rho(\mathbf{r})(3z^2 - r^2)d\mathbf{r},$$
$$R_g^2 = \frac{1}{N}\int \rho(\mathbf{r})r^2 d\mathbf{r},$$

where the continuous integration over the fluid density $\rho(\mathbf{r})$ should be replaced by a discrete summation over atoms with ZPAD, or replica beads with RPMD. Figure 6 shows the variations of the quantity Q_{zz}/R_g^2 predicted by the various methods, as a function of time and, for the particle-based methods, after averaging over independent trajectories.

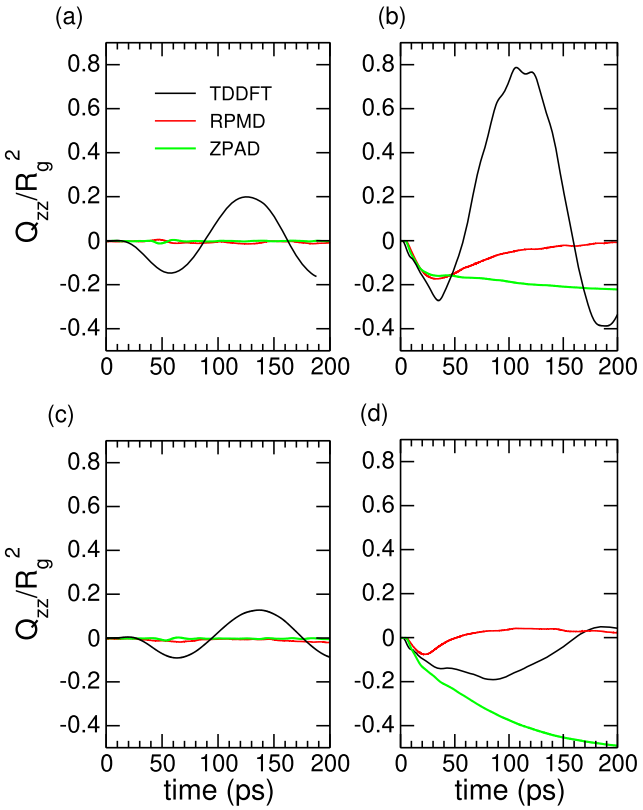

FIG. 6. Average quadrupole moment of the He_{1000} droplet undergoing a collision with a Cs atom as a function of time, as obtained with the RPMD, ZPAD, and TDDFT methods under different collision conditions. The RPMD and ZPAD results are averaged over 20 and 23 independent trajectories, respectively. (a) $b = 0$ and $v = 50$ m/s; (b) $b = 0$ and $v = 500$ m/s; (c) $b = 10$ Å and $v = 50$ m/s; (d) $b = 10$ Å and $v = 500$ m/s.

Here, again the influence of the collision velocity on the droplet shape is very significant. While the droplet remains nearly spherical for collisions at 50 m/s, head-on collisions at 500 m/s lead to significant deformations especially when modeled with the TDDFT method, in which piercing occurs.

Under such collision conditions, all methods predict quadrupole deformations of the oblate type, the droplet being compressed along the collision axis. However, within RPMD, the quadrupole deformation index, Q_{zz}/R_g^2, reaches a minimum after about 20 ps and, subsequently, the droplet relaxes toward a more spherical shape. The TDDFT approach predicts a qualitatively similar behavior for $b = 10$ Å, with the minimum of the quadrupole deformation being reached quite later, after about 100 ps. However, for head-on collisions, the deformation is much stronger with the droplet becoming significantly prolate after 100 ps and entering a seemingly oscillatory phase between the oblate and prolate shapes. With the ZPAD approach, the deformation begins similarly, but the droplet never really relaxes back to the spherical shape within the 200 ps time window, which is consistent with the slower dynamics experienced by these droplets in a more rigid-like state.

C. Merging of two He_{500} droplets

Coalescence[100] and splashing[33] experiments have demonstrated the liquid-like character of helium clusters at the experimental temperatures, a crucial feature to account for the suitability of helium droplets as carrier species in soft-landing processes.[33,36] Quite remarkably, the sequence of droplet shapes representative of the coalescence of two He droplets has been found to resemble that obtained upon merging of two classical drops,[101] and a close analogy has also been undertaken between the coalescence of superfluid He droplets and that of ultradilute quantum droplets, made of mixtures of ultracold ^{39}K atoms in different hyperfine states of a self-bound Bose–Einstein condensate.[102,103]

The merging, or coalescence, between two He_{500} clusters brought into contact is driven by their mutual van der Waals attraction, without the need for imposing relative velocities to the clusters. This process has been investigated using the density-based TDDFT approach in recent years,[62,63] and in the present work, we have carried out a complementary exploration of this process using the particle-based RPMD and ZPAD methods. Here also, several independent trajectories were performed, after which the physical properties were determined and averaged.

It is instructive to first consider the qualitative picture that emerges from these simulations. Figure 7 compares the shapes of the merging droplets, as predicted by the TDDFT, RPMD, and ZPAD methods, as a function of time with three snapshots selected at the beginning ($t = 0$) and after 100 or 200 ps. From a more quantitative perspective, the normalized quadrupole deformation parameter Q_{zz}/R_g^2 is also shown in the graph of Fig. 7 as a function of time.

The three approaches predict rather contrasted behaviors, which are nonetheless consistent with the shape analysis performed in the case of collisions with the Cs projectile. With the RPMD method, the merging proceeds in a mostly steady way, the newly formed droplet becoming more and more spherical over time in ~200 ps. With ZPAD, merging is hindered due to the individual

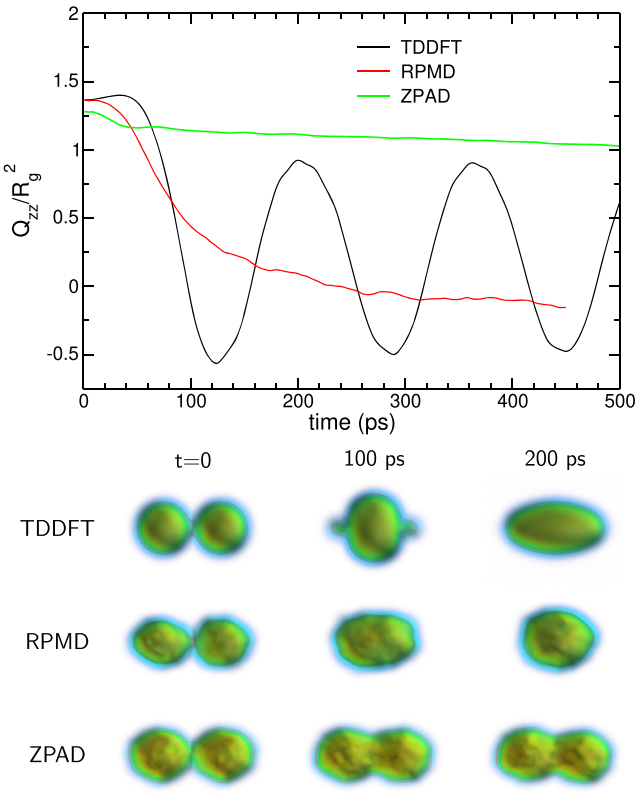

FIG. 7. Upper panel: Quadrupole deformation of the two He_{500} droplets merging upon contact, as predicted by the RPMD, ZPAD, and TDDFT methods, as a function of time. The RPMD and ZPAD results are averaged over 10 and 13 independent trajectories, respectively. Lower panel: Instantaneous shapes of two He_{500} droplets undergoing spontaneous merging upon contact, as predicted by the RPMD, ZPAD, and TDDFT methods, at $t = 0$ and after 100 and 200 ps.

droplets being insufficiently soft and mostly crystalline. Extending the trajectories to time scales reaching 1 ns does not improve the results significantly. The density-based approach predicts deformations that even exceed those found with RPMD, but in the absence of viscous damping, the superfluid droplet that experiences merging actually changes back and forth between oblate and prolate shapes through a slow oscillatory motion with a period of about 150 ps, which roughly corresponds to the quadrupole oscillation period of a He_{1000} droplet.

IV. CONCLUDING REMARKS

The formation of complexes or clusters inside helium nanodroplets is faced with two seemingly contradictory mechanisms. The extreme fluid character of helium itself is expected not to hinder the motion of the atomic or molecular partners much once inside the droplet. However, due to the cryogenic temperatures that are imposed by the droplet itself, rearrangements can be excessively slow and the complexes may also be stuck in metastable structures that are entropically favored, as shown experimentally by a number of studies.[10,11,15,16] Direct bonds can also be prevented from forming because of the high density of the helium solvation shell around heliophilic atoms.[20,22,32]

Because the complexes cannot be entirely explained by equilibrium thermodynamics considerations, it is important that any attempt at modeling complex formation in helium droplets incorporates dynamical effects as much as possible. In the present work, three complementary approaches were employed to address the time-dependent processes of cluster formation through sequential pickup, focusing on the addition of an argon atom on a preformed argon cluster embedded in a He_{1000}, helium droplet a more realistic situation complementary to the very symmetric ones explored in earlier TDDFT studies.[32] The same methods were then used to study the contrasted situation of the heliophobic cesium atom impinging on pristine droplets, as well as the spontaneous merging between two smaller He_{500} droplets put into contact and driven by long-range van der Waals forces.

The three methodologies followed here consist of the density-based TDDFT approach, the particle-based ZPAD approach, and the path-integral RPMD method, which also relies on a particle description but lies somewhat in between the two other approaches through the physical extension of the polymer beads associated with each atom. While TDDFT also accounts for the superfluid character of the helium droplets, only zero-point delocalization is incorporated in the two particle-based methods, and in ZPAD, these effects are treated empirically by attaching a frozen wavefunction to each He atom, determined iteratively at the desired temperature of 0.38 K, resulting in classical dynamics of the He atoms with effective potentials.

Regarding the coagulation process between heliophilic argon atoms, the three methods predict qualitatively similar behaviors in regard to various important aspects: The impinging argon always enters the droplet, but most of the time, the thermodynamically most stable isomer is not formed. Instead, metastable structures are formed and prevented to relax to the unique minima by their low kinetic energy associated with a shell structure of helium built around them. The methods differ in that the particle-based methods require a higher impact velocity in order to form a dimer, presumably because of the lack of superfluidity.

In the case of a heliophobic cesium atom impinging on a bare $^4He_{1000}$ droplet, all three methods find the Cs atom to be captured at the lower collision velocity (50 m/s). Differences arise at the higher velocity of 500 m/s: The density-based approach finds the projectile to pierce through the droplet, whereas both particle-based methods predict that it should be mostly captured or occasionally scattered (ZPAD). This difference could be again attributed to the superfluid behavior, most notably since the velocity of the outgoing Cs atom is found to be similar to the critical Landau velocity for the functional used in this work.

The merging between two small droplets also shows some qualitative differences that shed further light onto the possible importance of superfluidity and delocalization effects in the way they are included (or ignored) from the three methods. In the absence of viscous dissipation, TDDFT predicts large amplitude quadrupole oscillations for the merged He_{1000} droplet, while RPMD predicts a rather continuous process where the merged droplet becomes increasingly spherical. Due to the excessive solid-like character predicted by ZPAD, this process appears particularly slow with this method.

While TDDFT is, in principle, more realistic in describing the superfluid droplets, and even though thermal effects are expected to be limited under the relevant experimental conditions, as a zero temperature method it also ignores the possible fluctuations that, e.g., the doping complexes could experience inside the droplet. The main limitation of TDDFT is that it is significantly more time-consuming than both particle-based approaches, hampering systematic studies as the spatial and temporal resolutions of the TDDFT equations have to be adjusted to the nature of the dopant and the collision velocity. As such, it would not have been thinkable of modeling the collision process onto droplets containing argon clusters that are randomly oriented, only symmetric directions being chosen here for the sake of illustration.

In contrast, the ZPAD method provides a computationally very efficient way of simulating the doped helium droplets, once the effective potentials have been obtained. In particular, accounting for the statistics due to different orientations of the target cluster is straightforward, as well as extending trajectories to the nanosecond time scale or even beyond. It can also predict nonadiabatic transitions in the electronically excited dopant, when used in combination with mixed quantum–classical dynamics for the latter.[55–57] In addition, the internal temperature is equal to that of the experimental droplets (0.38 K). Its main limitation is its key dependence on the effective potentials (especially the He–He potential), which was found here to be probably too deep as it leads to droplets that are not actually liquid. This points to the need for a specific criterion to fix the truncation distance of the effective He wavefunction.

The RPMD approach is intermediate between the TDDFT and ZPAD methods, at least in terms of computational cost, which increases linearly with the Trotter discretization number. While we do not expect any qualitative improvement of the method with increasing this number (or lowering the temperature down to experimental values), it would be worth considering thermostated versions of the algorithm[104] in the future so even higher numbers of replica beads could be employed. This would notably clarify some of the differences noted with the density-based method, like the motion of argon impurities inside the helium droplet that might be ascribable to the higher temperature of 1 K employed within RPMD. Yet the method can also account for statistics, at least to a reasonable extent, although the trajectories can hardly be as long as those with ZPAD.

To some extent, RPMD can be said to provide information about the importance of superfluidity when compared to TDDFT and about the importance of fluid-like effects in themselves when compared to ZPAD in its current version. The lack of bosonic exchange effects in the particle-based approaches likely explains the qualitative differences found in the high-velocity capture (or absence thereof) of the Cs atom onto the droplets, or the quadrupole oscillations in the merging process, which reveals or stresses what is essentially due to superfluidity in these processes. However, the more approximate methods are suited to address cases where superfluidity may not be essential, especially if the interaction between the dopant and the helium host is strong or when the processes taking place are highly energetic. An extreme case would be that of ionic dopants, where the local crystallization of the solvent in their vicinity (usually referred to as a snowball effect) could be more difficult to address dynamically with density-based methods because of the numerical constraints on the time and space steps that the rapidly varying densities would practically impose.

SUPPLEMENTARY MATERIAL

See the supplementary material for the analytical expression of the effective Ar–He and He–He ZPAD potentials, as well as the corresponding parameters, with a figure comparing this potential to the reference interactions. Selected videos showing typical trajectories obtained with the various methods and for the different systems are also provided.

ACKNOWLEDGMENTS

This work has been performed under Grant No. PID2020-114626GB-I00 from the MICIN/AEI/10.13039/501100011033. M.B. acknowledges the Université Fédérale Toulouse Midi-Pyrénées for financial support throughout the "Chaires d'Attractivité 2014" Programme IMDYNHE. E.G.-A. acknowledges financial support from the same program. The authors gratefully acknowledge the regional computer center of Midi-Pyrénées, CALMIP (Grant No. P1039), the regional computer center of Champagne-Ardenne, ROMEO, and the Pôle Scientifique de Modélisation Numérique (PSMN) in Lyon, for providing high performance computer resources.

AUTHOR DECLARATIONS

Conflict of Interest

The authors have no conflicts to disclose.

Author Contributions

Ernesto García-Alfonso: Data curation (equal); Investigation (equal). **Manuel Barranco:** Conceptualization (equal); Data curation (equal); Formal analysis (equal); Investigation (equal); Methodology (equal); Project administration (equal); Supervision (equal); Validation (equal); Writing – original draft (equal); Writing – review and editing (equal). **David A. Bonhommeau:** Conceptualization (equal); Data curation (equal); Investigation (equal); Methodology (equal); Supervision (equal); Validation (equal); Writing – original draft (equal); Writing – review and editing (equal). **Nadine Halberstadt:** Conceptualization (equal); Data curation (equal); Investigation (equal); Methodology (equal); Supervision (equal); Validation (equal); Writing – original draft (equal); Writing – review and editing (equal). **Martí Pi:** Conceptualization (equal); Data curation (equal); Investigation (equal); Supervision (equal); Validation (equal); Writing – original draft (equal); Writing – review and editing (equal). **Florent Calvo:** Conceptualization (equal); Data curation (equal); Investigation (equal); Methodology (equal); Project administration (equal); Supervision (equal); Validation (equal); Writing – original draft (equal); Writing – review and editing (equal).

DATA AVAILABILITY

The data that support the findings of this study are available from the corresponding author upon reasonable request.

REFERENCES

[1] J. P. Toennies and A. F. Vilesov, Angew. Chem., Int. Ed. **43**, 2622 (2004).
[2] A. Scheidemann, J. P. Toennies, and J. A. Northby, Phys. Rev. Lett. **64**, 1899 (1990).
[3] K. K. Lehmann and G. Scoles, Science **279**, 2065 (1998).
[4] M. Y. Choi, G. E. Douberly, T. M. Falconer, W. K. Lewis, C. M. Lindsay, J. M. Merritt, P. L. Stiles, and R. E. Miller, Int. Rev. Phys. Chem. **25**, 15 (2006).
[5] C. Callegari and W. E. Ernst, in *Handbook of High Resolution Spectroscopy* (Wiley, New York, 2011), Vol. 3, p. 1551.
[6] M. Mudrich and F. Stienkemeier, Int. Rev. Phys. Chem. **33**, 301 (2014).
[7] J. Tiggesbäumker and F. Stienkemeier, Phys. Chem. Chem. Phys. **9**, 4748 (2007).
[8] A. Mauracher, O. Echt, A. M. Ellis, S. Yang, D. K. Bohme, J. Postler, A. Kaiser, S. Denifl, and P. Scheier, Phys. Rep. **751**, 1 (2018).
[9] W. E. Ernst and A. W. Hauser, Phys. Chem. Chem. Phys. **23**, 7553 (2021).
[10] K. Nauta and R. E. Miller, Science **283**, 1895 (1999).
[11] E. Loginov, L. F. Gomez, N. Chiang, A. Halder, N. Guggemos, V. V. Kresin, and A. F. Vilesov, Phys. Rev. Lett. **106**, 233401 (2011).
[12] J. D. Pickering, B. Shepperson, L. Christiansen, and H. Stapelfeldt, J. Chem. Phys. **149**, 154306 (2018).
[13] K. Nauta and R. E. Miller, Science **287**, 293 (2000).
[14] J. Khatri, T. K. Roy, K. Chatterjee, G. Schwaab, and M. Havenith, J. Phys. Chem. A **125**, 6954 (2021).
[15] E.-M. Lottner and A. Slenczka, J. Phys. Chem. A **124**, 311 (2020).
[16] A. M. Ellis, J. A. Davies, E. Yurtsever, and F. Calvo, J. Chem. Phys. **156**, 174304 (2022).
[17] V. Mozhayskiy, M. N. Slipchenko, V. K. Adamchuk, and A. F. Vilesov, J. Chem. Phys. **127**, 094701 (2007).
[18] G. Haberfehler, P. Thaler, D. Knez, A. Volk, F. Hofer, W. E. Ernst, and G. Kothleitner, Nat. Commun. **6**, 8779 (2015).
[19] A. Volk, P. Thaler, D. Knez, A. W. Hauser, J. Steurer, W. Grogger, F. Hofer, and W. E. Ernst, Phys. Chem. Chem. Phys. **18**, 1451 (2016).
[20] J. Eloranta, Phys. Rev. B **77**, 134301 (2008).
[21] A. Przystawik, S. Göde, T. Döppner, J. Tiggesbäumker, and K.-H. Meiwes-Broer, Phys. Rev. A **78**, 021202(R) (2008).
[22] A. Hernando, M. Barranco, R. Mayol, M. Pi, and F. Ancilotto, Phys. Rev. B **78**, 184515 (2008).
[23] L. F. Gomez, E. Loginov, and A. F. Vilesov, Phys. Rev. Lett. **108**, 155302 (2012).
[24] E. Latimer, D. Spence, C. Feng, A. Boatwright, A. M. Ellis, and S. Yang, Nano Lett. **14**, 2902 (2014).
[25] P. Thaler, A. Volk, F. Lackner, J. Steurer, D. Knez, W. Grogger, F. Hofer, and W. E. Ernst, Phys. Rev. B **90**, 155442 (2014).
[26] J. Gspann and H. Vollmar, J. Chem. Phys. **73**, 1657 (1980).
[27] J. Gspann and R. Ries, Surf. Sci. **156**, 195 (1985).
[28] J. P. Toennies, The Chemical Physics of Atomic and Molecular Clusters, in *Proceedings of the International School of Physics "Enrico Fermi" Course CVII*, edited by G. Scoles (North Holland, Amsterdam, 1990), p. 597.
[29] D. Eichenauer, A. Scheidemann, and J. P. Toennies, Z. Phys. D **8**, 295 (1988).
[30] M. Lewerenz, B. Schilling, and J. P. Toennies, J. Chem. Phys. **102**, 8191 (1995).
[31] F. Coppens, F. Ancilotto, M. Barranco, N. Halberstadt, and M. Pi, Phys. Chem. Chem. Phys. **19**, 24805 (2017).
[32] F. Coppens, F. Ancilotto, M. Barranco, N. Halberstadt, and M. Pi, Phys. Chem. Chem. Phys. **21**, 17423 (2019).
[33] P. Martini, S. Albertini, F. Laimer, M. Meyer, M. Gatchell, O. Echt, F. Zappa, and P. Scheier, Phys. Rev. Lett. **127**, 263401 (2021).
[34] N. F. Aguirre, D. Mateo, A. O. Mitrushchenkov, M. Pi, and M. P. de Lara-Castells, J. Chem. Phys. **136**, 124703 (2012).
[35] M. P. de Lara-Castells, N. F. Aguirre, H. Stoll, A. O. Mitrushchenkov, D. Mateo, and M. Pi, J. Chem. Phys. **142**, 131101 (2015).
[36] R. Fernández-Perea, L. F. Gómez, C. Cabrillo, M. Pi, A. O. Mitrushchenkov, A. F. Vilesov, and M. P. de Lara-Castells, J. Phys. Chem. C **121**, 22248 (2017).
[37] R. B. Gerber and M. A. Ratner, Adv. Chem. Phys. **70**, 97 (1988).
[38] J. M. Bowman, K. Christoffel, and F. Tobin, J. Phys. Chem. **83**, 905 (1979).
[39] V. Buch, J. Chem. Phys. **117**, 4738 (2002).
[40] P. A. Frantsuzov and V. A. Mandelshtam, J. Chem. Phys. **128**, 094304 (2008).
[41] M. Barranco, R. Guardiola, S. Hernández, R. Mayol, J. Navarro, and M. Pi, J. Low Temp. Phys. **142**, 1 (2006).
[42] F. Ancilotto, M. Barranco, F. Coppens, J. Eloranta, N. Halberstadt, A. Hernando, D. Mateo, and M. Pi, Int. Rev. Phys. Chem. **36**, 621 (2017).
[43] F. Dalfovo, A. Lastri, L. Pricaupenko, S. Stringari, and J. Treiner, Phys. Rev. B **52**, 1193 (1995).
[44] F. Ancilotto, M. Barranco, F. Caupin, R. Mayol, and M. Pi, Phys. Rev. B **72**, 214522 (2005).
[45] A. Leal, D. Mateo, A. Hernando, M. Pi, and M. Barranco, Phys. Chem. Chem. Phys. **16**, 23206 (2014).
[46] A. Vilà and M. González, Phys. Chem. Chem. Phys. **18**, 31869 (2016).
[47] F. Coppens, A. Leal, M. Barranco, N. Halberstadt, and M. Pi, J. Low Temp. Phys. **187**, 439 (2017).
[48] M. Blancafort-Jorquera, A. Vilà, and M. González, Phys. Chem. Chem. Phys. **20**, 29737 (2018).
[49] M. Blancafort-Jorquera, A. Vilà, and M. González, Phys. Chem. Chem. Phys. **21**, 24218 (2019).
[50] I. R. Craig and D. E. Manolopoulos, J. Chem. Phys. **121**, 3368 (2004).
[51] A. Castillo-García, A. W. Hauser, M. P. de Lara-Castells, and P. Villarreal, Molecules **26**, 5783 (2021).
[52] F. Calvo, E. Yurtsever, and Ö. Birer, J. Phys. Chem. A **120**, 1727 (2016).
[53] E. J. Heller, J. Chem. Phys. **75**, 2923 (1981).
[54] M. Sterling, Z. Li, and V. A. Apkarian, J. Chem. Phys. **103**, 5679 (1995).
[55] D. Bonhommeau, P. T. Lake, Jr., C. Le Quiniou, M. Lewerenz, and N. Halberstadt, J. Chem. Phys. **126**, 051104 (2007).
[56] D. Bonhommeau, M. Lewerenz, and N. Halberstadt, J. Chem. Phys. **128**, 054302 (2008).
[57] N. Halberstadt and D. A. Bonhommeau, J. Chem. Phys. **152**, 234305 (2020).
[58] C. Stark and V. V. Kresin, Phys. Rev. B **81**, 085401 (2010).
[59] L. A. der Lan, P. Bartl, C. Leidlmair, H. Schöbel, R. Jochum, S. Denifl, T. D. Märk, A. M. Ellis, and P. Scheier, J. Chem. Phys. **135**, 044309 (2011).
[60] L. A. der Lan, P. Bartl, C. Leidlmair, H. Schöbel, S. Denifl, T. D. Märk, A. M. Ellis, and P. Scheier, Phys. Rev. B **85**, 115414 (2012).
[61] F. Calvo, Phys. Rev. B **95**, 035429 (2017).
[62] J. M. Escartín, F. Ancilotto, M. Barranco, and M. Pi, Phys. Rev. B **105**, 024511 (2022).
[63] J. M. Escartín, F. Ancilotto, M. Barranco, and M. Pi, Phys. Rev. B **99**, 140505(R) (2019).
[64] M. Barranco, F. Coppens, N. Halberstadt, A. Hernando, A. Leal, D. Mateo, R. Mayol, and M. Pi, "Zero temperature DFT and TDDFT for ^{4}He: A short guide for practitioners," 2017, https://github.com/bcntls2016/DFT-Guide/blob/master/dft-guide.pdf.
[65] A. Wada, T. Takayanagi, and M. Shiga, J. Chem. Phys. **119**, 5478 (2003).
[66] T. Takayanagi and M. Shiga, Phys. Chem. Chem. Phys. **6**, 3241 (2004).
[67] S. Stringari and J. Treiner, J. Chem. Phys. **87**, 5021 (1987).
[68] D. J. Wales, J. P. K. Doye, A. Dullweber, M. P. Hodges, F. Y. Naumkin, F. Calvo, J. Hernández-Rojas, and T. F. Middleton, The Cambridge Cluster Database, http://www-wales.ch.cam.ac.uk/CCD.html.
[69] J. Höller, E. Krotscheck, and R. E. Zillich, Eur. Phys. J. D **68**, 372 (2014).
[70] J. Höller, E. Krotscheck, and R. E. Zillich, Eur. Phys. J. D **69**, 198 (2015).
[71] K. T. Tang and J. P. Toennies, J. Chem. Phys. **118**, 4976 (2003).
[72] S. H. Patil, J. Chem. Phys. **94**, 8089 (1991).
[73] M. Pi, F. Ancilotto, F. Coppens, N. Halberstadt, A. Hernando, A. Leal, D. Mateo, R. Mayol, and M. Barranco, "^{4}He-DFT BCN-TLS: A computer package for simulating structural properties and dynamics of doped liquid helium-4 systems," https://github.com/bcntls2016/.
[74] M. Frigo and S. G. Johnson, Proc. IEEE **93**, 216 (2005).
[75] A. Ralston and H. S. Wilf, *Mathematical Methods for Digital Computers* (John Wiley & Sons, New York, 1960).
[76] T. J. H. Hele and S. C. Althorpe, J. Chem. Phys. **138**, 084108 (2013).
[77] T. J. H. Hele, M. J. Willatt, A. Muolo, and S. C. Althorpe, J. Chem. Phys. **142**, 191101 (2015).

[78]S. Habershon, G. S. Fanourgakis, and D. E. Manolopoulos, J. Chem. Phys. **129**, 074501 (2009).
[79]M. Shiga and A. Nakayama, Chem. Phys. Lett. **451**, 175 (2008).
[80]F. Calvo, P. Parneix, and N.-T. Van-Oanh, J. Chem. Phys. **132**, 124308 (2010).
[81]S. Habershon, T. E. Markland, and D. E. Manolopoulos, J. Chem. Phys. **131**, 024501 (2009).
[82]F. Calvo and D. Costa, J. Chem. Theory Comput. **6**, 508 (2010).
[83]R. Collepardo-Guevara, Y. V. Suleimanov, and D. E. Manolopoulos, J. Chem. Phys. **130**, 174713 (2009).
[84]A. R. Menzeleev, F. Bell, and T. F. Miller III, J. Chem. Phys. **140**, 064103 (2014).
[85]A. R. Menzeleev and T. F. Miller III, J. Chem. Phys. **132**, 034106 (2010).
[86]F. Calvo, C. Falvo, and P. Parneix, J. Phys. Chem. A **118**, 5427 (2014).
[87]R. Welsch, K. Song, Q. Shi, S. C. Althorpe, and T. F. Miller III, J. Chem. Phys. **145**, 204118 (2016).
[88]M. Tuckerman, B. J. Berne, and G. J. Martyna, J. Chem. Phys. **97**, 1990 (1992).
[89]T. E. Markland and D. E. Manolopoulos, J. Chem. Phys. **129**, 024105 (2008).
[90]P. Slavíček, P. Jungwirth, M. Lewerenz, N. H. Nahler, M. Fárník, and U. Buck, J. Phys. Chem. A **107**, 7743 (2003).
[91]D. A. Bonhommeau, Chem. Phys. **550**, 111307 (2021).
[92]R. Panzou and M. Lewerenz, Mol. Phys. **119**, e1977862 (2021).
[93]F. Ancilotto, M. Pi, R. Mayol, M. Barranco, and K. K. Lehmann, J. Phys. Chem. A **111**, 12695 (2007).
[94]A. Leal, D. Mateo, A. Hernando, M. Pi, M. Barranco, A. Ponti, F. Cargnoni, and M. Drabbels, Phys. Rev. B **90**, 224518 (2014).
[95]M. Lewerenz, B. Schilling, and J. P. Toennies, Chem. Phys. Lett. **206**, 381 (1993).
[96]M. Theisen, F. Lackner, and W. E. Ernst, J. Chem. Phys. **135**, 074306 (2011).
[97]S. M. O. O'Connell, R. M. P. Tanyag, D. Verma, C. Bernando, W. Pang, C. Bacellar, C. A. Saladrigas, J. Mahl, B. W. Toulson, Y. Kumagai, P. Walter, F. Ancilotto, M. Barranco, M. Pi, C. Bostedt, O. Gessner, and A. F. Vilesov, Phys. Rev. Lett. **124**, 215301 (2020).
[98]M. Pi, J. M. Escartín, F. Ancilotto, and M. Barranco, Phys. Rev. B **104**, 094509 (2021).
[99]N. B. Brauer, S. Smolarek, E. Loginov, D. Mateo, A. Hernando, M. Pi, M. Barranco, W. J. Buma, and M. Drabbels, Phys. Rev. Lett. **111**, 153002 (2013).
[100]C. L. Vicente, C. Kim, H. J. Maris, and G. M. Seidel, J. Low Temp. Phys. **121**, 627 (2000).
[101]J. Qian and C. K. Law, J. Fluid Mech. **331**, 59 (1997).
[102]G. Ferioli, G. Semeghini, L. Masi, G. Giusti, G. Modugno, M. Inguscio, A. Gallemí, A. Recati, and M. Fattori, Phys. Rev. Lett. **122**, 090401 (2019).
[103]V. Cikojević, L. V. Markić, M. Pi, M. Barranco, F. Ancilotto, and J. Boronat, Phys. Rev. Res. **3**, 043139 (2021).
[104]M. Ceriotti, M. Parrinello, T. E. Markland, and D. E. Manolopoulos, J. Chem. Phys. **133**, 124104 (2010).